Improving Arctic sea-ice thickness estimates with the assimilation of CryoSat-2 summer observations

Chao Min[1,2], Qinghua Yang[1], Hao Luo[1], Jack C. Landy[3], Dake Chen[1], Geoffrey J. Dawson[4], Thomas Krumpen[2], Nabir Mamnun[2], Xiaoyu Liu[2], and Lars Nerger[2]

[1]School of Atmospheric Sciences, Sun Yat-sen University, and Southern Marine Science and Engineering Guangdong Laboratory (Zhuhai), Zhuhai, China.

[2]Alfred Wegener Institute, Helmholtz Centre for Polar and Marine Research, Bremerhaven, Germany.

[3]Centre for Integrated Remote Sensing and Forecasting for Arctic Operations, Department of Physics and Technology, University of Tromsø The Arctic University of Norway, Tromsø, Norway.

[4]Bristol Glaciology Centre, School of Geographical Sciences, University of Bristol, Bristol, UK.

Corresponding author: Qinghua Yang (yangqh25@mail.sysu.edu.cn)

Key Points:

- CryoSat-2 summer sea-ice thickness (SIT) is assimilated into a coupled ice-ocean model for the first time.
- The discontinuity brought by assimilating biweekly CryoSat-2 SIT is overcome by implementing an incremental analysis update scheme.
- Significant improvements in sea-ice estimates are obtained in the areas where the sea ice is roughest and experiences strong deformation.

Abstract

Rapidly shrinking Arctic sea ice has had significant impacts on the Arctic Ocean and many outer Arctic regions. It is therefore urgently needed to reliably estimate Arctic sea-ice thickness (SIT) by combined use of available observation and numerical modeling. Here, for the first time, we assimilate the latest CryoSat-2 summer SIT data into a coupled ice-ocean model. In particular, an Incremental Analysis Update scheme is implemented to overcome the discontinuity brought by assimilating biweekly SIT and daily sea ice concentration data. Along with an improvement in sea ice volume, our SIT estimates have smaller errors than that without SIT assimilation in areas where the sea ice is roughest and experiences strong deformation, e.g., around the Fram Strait and Greenland. This study suggests that the newly-developed CryoSat-2 SIT product, when assimilated properly with our approach, has great potential for Arctic sea ice simulation and prediction.

Plain Language Summary

In this study, we incorporate the latest biweekly summer sea-ice thickness (SIT) and daily sea-ice concentration (SIC) data from satellite observations into an ice-ocean model to improve the model estimates. Data assimilation (DA) is used here for combining observational data with model simulation. Summer SIT was not assimilated into ice-ocean models before this study. We find better results when we use SIC and summer SIT observations simultaneously with the DA technique than using SIC only. Significant improvements in the SIT field are found in the areas where the sea ice is roughest and experiences strong deformation. This study provides a promising perspective for applying the latest satellite observations of summer SIT to sea ice estimating and forecasting.

1 Introduction

Coinciding with a four-fold Arctic warming ratio compared to the globe on average (Chylek et al., 2022; Rantanen et al., 2022), Arctic sea ice has declined sharply during the satellite era (Kwok, 2018; Stroeve & Notz, 2018). The substantial sea ice loss has significantly influenced the Earth system (Bailey et al., 2021; Cohen et al., 2021; Liu et al., 2022; Qi et al., 2022). For instance, Arctic sea ice reduction is likely linked to extreme events in the middle and lower latitudes (Bailey et al., 2021; Cohen et al., 2021; Liu et al., 2022). Although the ongoing decline has made commercial trans-Arctic transit more feasible in the summer, the changing and

mobile sea ice impacts maritime activities (e.g., Eicken, 2013; Min, et al., 2022). For instance, local variations in sea-ice thickness (SIT) can affect the safety and route-planning decisions of maritime navigators. Consequently, there is a great need and interest in reliable measurements, simulations and forecasts of Arctic sea ice.

Sophisticated year-round sea-ice concentration (SIC) monitoring has been developed for several decades (e.g., Comiso et al., 1997; Lavergne et al., 2019; Spreen et al., 2008). SIT data like SMOS (Kaleschke et al., 2012; Tian-Kunze et al., 2014), CryoSat-2 (Laxon et al., 2013; Ricker et al., 2014), and ICESat-2 (Kwok et al., 2020; Petty et al., 2020) were enhanced over the year, but have been only available during winter. Recently, a pan-Arctic summer SIT product derived from CryoSat-2 has become available (Landy et al., 2022). The most recent CryoSat-2 summer SIT data not only offers the first look at Arctic SIT from the perspective of satellite remote sensing but also unlocks opportunities for constructing a more reliable SIT reanalysis by assimilating this data into dynamical models and generating sea-ice forecasts (Landy et al., 2022).

Data assimilation (DA) is highly effective in enhancing sea-ice estimates because the model initialization can be adjusted and the model state can continuously be constrained to reality by integrating new observations (Blockley & Peterson, 2018; Day et al., 2014; Massonnet et al., 2015). The assimilation of winter SIT, for instance, can provide improved initial conditions for the summer season and hence has the potential to lower uncertainty in both sea-ice estimates and forecasts (e.g., Blockley & Peterson, 2018; Day et al., 2014; Mignac et al., 2022; Xie et al., 2018; Yang et al., 2014; Yang et al., 2019). In particular, to improve the ice-thickness estimates, a year-round Combined Model and Satellite Thickness (CMST) reanalysis has been developed by assimilating the CryoSat-2 and SMOS thickness data throughout the freezing season Mu, Losch, et al., 2018). Although CMST has been systematically evaluated and widely used (e.g., Li et al., 2022; Min et al., 2019; Min et al., 2021; Mu, Losch, et al., 2018; Zhou et al., 2021), the SIT is only corrected indirectly in summer through the positive covariance between SIC, which is assimilated, and SIT, which is not during the summer months. Moreover, the weekly mean SIT from CryoSat-2 is simply assimilated every day of the week during the cold season (Mu, Losch, et al., 2018; Mu, Yang, et al., 2018), which may introduce unphysical "jumps" at the transition of different weeks and seasons (i.e., winter-summer and summer-winter). To date, there has not been a study focusing on the impact and approach of assimilating

satellite-based summer SIT. Given the current availability of summer SIT data, we conduct a DA experiment by simultaneously assimilating summer SIC and SIT.

This study aims to explore whether the assimilation of CryoSat-2 summer SIT data can better constrain modeled SIC and SIT and thus improve sea-ice estimates. We applied an Incremental Analysis Update (IAU) scheme for CryoSat-2 summer SIT assimilation to ensure the physical development of sea-ice volume (SIV) and SIT with CryoSat-2 observations available at a lower biweekly time interval compared to daily SIC observations. We further compare our outputs with CMST and different independent data to assess the overall improvement by assimilating summer SIT.

2 Materials and Methods

2.1 Satellite-retrieved observations

The pan-Arctic year-round CryoSat-2 SIT dataset has been generated by combining deep learning radar waveform classification with numerical radar simulations (Landy et al., 2022). In summary, a one-dimensional convolutional neural network (CNN) has been applied to classify leads from sea-ice returns in radar altimeter waveforms (Dawson et al., 2022). A series of numerical waveform simulations based on the Facet-Based Echo Model (Landy et al., 2020; Landy et al., 2019), which integrates melt ponds, are then used to calibrate a radar range bias that causes the CryoSat-2 freeboards to be underestimated. The SIT is derived from CryoSat-2 radar freeboards assuming hydrostatic equilibrium and accounting for snow loading, with snow depth and density estimates obtained from SnowModel-LG (https://nsidc.org/data/nsidc-0758/versions/1; Stroeve et al., 2020). The innovative dataset provides SIT and its uncertainty with a temporal resolution of 15 or 16 days and a spatial resolution of 80 km. Large uncertainties still remain, nevertheless, close to the coast of northern Greenland and the Fram Strait when compared to airborne electromagnetic (AEM) thickness observations (Landy et al., 2022). More details about data processing can be found in Dawson et al. (2022) and Landy et al. (2022).

The SIC data used in this study is computed at the French Research Institute for Exploitation of the Sea (IFREMER) and reprocessed by the Integrated Climate Data Center. Together with the ARTIST Sea Ice algorithm (Kaleschke et al., 2001; Spreen et al., 2008), this SIC dataset is derived from brightness temperatures measured with the 85-GHz Special Sensor Microwave / Imager (SSM/I) and/or Special Sensor Microwave / Imager Sounder (SSM/IS)

channels. A 5-day median filter is used to reduce unrealistic short-term SIC variations resulting from weather influence (Kern et al., 2010). The spatial resolution of the daily SIC data is 12.5 km.

2.2 Reference observations

The sea-ice extents (SIEs) estimated from CMST and our experiments are evaluated using the SIC observation that is processed by the NASA team algorithm and distributed by National Snow and Ice Data Center (NSIDC, DiGirolamo et al., 2022). This independent SIC dataset is used to ensure we are not assimilating and testing against the same observations. Moreover, to validate the SIT results, we use a set of independent fixed mooring and airborne sea ice thickness observations (see Fig. 1 for geographic locations of surveys and deployment positions). Sea ice drafts were obtained from upward-looking sonars (ULS) provided by the Beaufort Gyre Experiment Program (BGEP) in 2015. Data from three different moorings are hereafter referred to as BGEP_A, BGEP_B and BGEP_D. According to Melling et al. (1995), the error associated with ULS sea ice draft observations is about 0.1 m. In addition, we used draft data based on an Acoustic Doppler Current Profiler (ADCP) deployed by the Alfred Wegener Institute (AWI) in the western Laptev Sea area in 2014. Following Belter et al. (2021), the uncertainties are relatively high (±0.96 m) but consistent. To simplify the comparison between model SIT and observations, the observed sea ice draft is converted to thickness by multiplying by a factor of 1.1 (Nguyen et al., 2011).

In addition to the moored observations, SIT from airborne electromagnetic (AEM) surveys (IceBird campaign) conducted by AWI in Fram Strait and northern Greenland (Krumpen et al., 2019) are used as a reference dataset for our model results. The applied surveys were conducted between 24 July and 1 August 2016 during the IceBird campaign. For more details on the methodology, we refer to Krumpen et al. (2020). According to Pfaffling et al. (2007), AEM observations are estimated to have an uncertainty of ±0.1 m over flat ice, although the accuracy may be affected by the presence of melt ponds. As the footprint of airborne measurements is in the range of tens of meters, all AEM-based SIT are averaged onto the CroSat-2 grids for comparison, following Landy et al. (2022). As the numerical model carries the effective/mean ice thickness (volume over an area), all field observations are multiplied by the local NSIDC SIC

144 to obtain the observed mean thickness to facilitate the comparison between the model and
145 observations following Yang et al. (2015).

146 **2.3 Sea-ice data assimilation system**

147 The DA system is further developed based on the CMST system. I.e., the Massachusetts
148 Institute of Technology general circulation model (MITgcm, Marshall et al., 1997) and the
149 Parallel Data Assimilation Framework (PDAF, Nerger & Hiller, 2013) are employed. The sea ice
150 dynamics use a viscous plastic rheology (Hibler, 1979; Zhang & Hibler, 1997), with a one-layer,
151 zero-heat capacity formulation applied in the thermodynamics (Parkinson & Washington, 1979;
152 Semtner, 1976). 50 vertical model layers are used in the ocean model, with 28 layers located in
153 the top 1000 m. An Arakawa C grid with a variable horizontal resolution with an average
154 spacing of 18 km, is used to discretize both the ocean and sea ice models. The experiments are
155 based on a regional MITgcm configuration with open boundaries located around 55°N in the
156 Atlantic and Pacific (Losch et al., 2010; Nguyen et al., 2011). Figure 1 depicts the model domain
157 with an orange mesh.

158 As with earlier DA studies (e.g., Mu, Losch, et al., 2018; Mu, Yang, et al., 2018; Yang et
159 al., 2015), the coupled ice-ocean model is driven by atmospheric ensemble forecasts generated
160 by the UK Met Office (UKMO) Ensemble Prediction System (EPS) and accessible from the
161 THORPEX Interactive Grand Global Ensemble archive (TIGGE) (Bowler et al., 2008; Park et al.,
162 2008) in order to incorporate flow-dependent uncertainty in atmospheric forcing. Eleven sets of
163 perturbed forecasts are employed to force an ensemble of eleven model states. Details about
164 atmospheric data processing can be found in previous works (Mu, Losch, et al., 2018; Yang et
165 al., 2015).

166 For easy comparison with the previously developed CMST reanalysis, which only
167 assimilates IFREMER SIC during summer, following Mu et al. (2018), the IFREMER SIC and
168 CryoSat-2 SIT are assimilated into the ice-ocean model by using the local error-subspace
169 transform Kalman filter (LESTKF) coded in PDAF (Nerger & Hiller, 2013; Nerger et al., 2012).
170 The LESTKF is a highly efficient ensemble Kalman filter with very high-dimensional models
171 (Nerger et al., 2012). SIC and SIT obtained from the forecast fields are stored together in the
172 state vector. Then, in each analysis step, the LESTKF is used to correct the state vector by only
173 taking into account the sea-ice data observed within a 126 km radius of each model point (Mu,

Losch, et al., 2018; Yang et al., 2015). The observations within the radius are weighted with distance from the grid point by a quasi-Gaussian weight function (Gaspari & Cohn, 1999). Model uncertainties are calculated from the ensemble of model states driven by the UKMO ensemble atmospheric forcing (Mu, Losch, et al., 2018; Yang et al., 2015). The observation error for SIC is set as a constant value of 0.25, while the variable SIT observation errors are provided by the CryoSat-2 dataset (Mu, Losch, et al., 2018; Yang et al., 2015).

For consistent pan-Arctic temporal and spatial coverage, the CryoSat-2 SIT data is available twice per month at an interval of 15 or 16 days (Landy et al., 2022; Lawrence et al., 2021). Therefore, the forecast interval between the analysis steps will be excessively long when assimilating CryoSat-2 data directly. The sparse analysis step typically creates unrealistically large "jumps" (increments) for the evolution of sea ice, leading to an unnatural development of SIV (figures are not shown). For forecasting systems that need daily updates, direct assimilation of this data is therefore inappropriate. Hence, an IAU strategy similar to previous studies (Bloom et al., 1996; Lellouche et al., 2013; Ourmières et al., 2006) is implemented to obtain smoother evolutions of sea ice. In brief, we run a 7-/8-day experiment that assimilates daily SIC and, when available, biweekly CryoSat-2 SIT. The SIT increment obtained at the analysis step that both SIC and SIT are assimilated is not applied immediately, but divided by each biweekly CryoSat-2's number of days, and stored for the IAU to make daily updates. Finally, the DA system is restarted assimilating daily SIC and incorporating daily SIT increments and producing the analysis fields. This approach allows us to assimilate the rather infrequent biweekly summer SIT data in combination with the daily SIC data, while ensuring a gradual development of the sea ice fields over time. A detailed description of the IAU scheme developed in this study is provided in Text S1 and Figure S1 in Supporting Information S1.

2.4 Experiment design

The beginning of 2016 experienced record-low monthly SIE but the summer extent exceeded most seasonal forecasts (Petty et al., 2017; Petty et al., 2018). Due to the unconsolidated summer ice cover in 2016, modeling and forecasting sea ice conditions during this summer are expected to be exceptionally challenging (Petty et al., 2017; Petty et al., 2018). Therefore, we carried out the DA experiment from May 23 to September 30, 2016. The performance of our experiments during the year 2016 is, therefore, a performance assessment

indicator of this system. Given that CMST data is already well-validated and applied (e.g., Li et al., 2022; Min et al., 2019; Min et al., 2021; Mu, Losch, et al., 2018; Zhou et al., 2021), following Yang et al (2019), restart files from this retrospective simulation (CMST) were used as the initial ice-ocean conditions for the DA experiments.

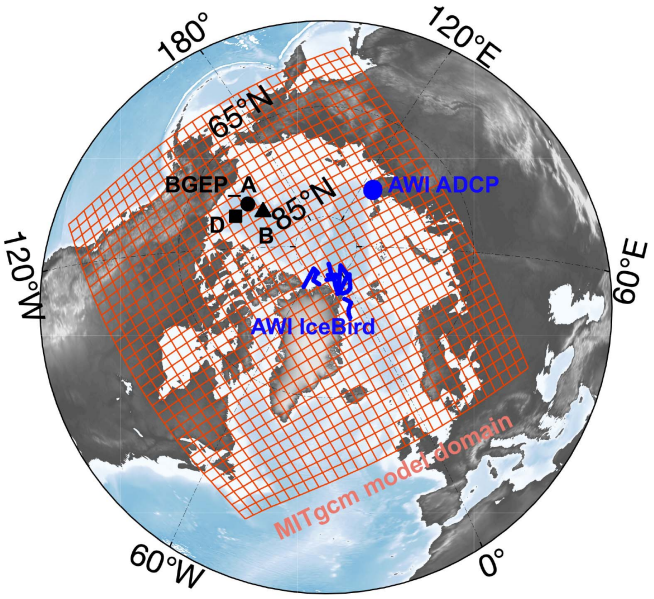

Figure 1. The MITgcm model grid is shown in an orange net plotted at every 12 model grid points. The independent observations used to validate CryoSat-2, Combined Model and Satellite Thickness (CMST) and the analysis field (ANA) are presented in blue extra-large dots for two AWI Acoustic Doppler Current Profiler (ADCP) sensor deployments, in blue lines for the AWI airborne surveys (IceBird), and in black dot, triangle and square for Beaufort Gyre Exploration Program (BGEP) moorings A, B and D, respectively. The blue dots for two AWI ADCPs (Vilk1-14 and Vilk3-14) are overlapped because of their near proximity.

3 Results

The spatial distributions of summer SIT are displayed in Figures 2a-2c and the daily evolution of SIE in Figure 2d and SIV in Figure 2e. Overall, the assimilation of summer SIT leads to a better agreement of the SIT and SIV estimated from our thickness analysis field (hereafter, ANA) with that from CryoSat-2 compared to CMST, which only assimilates SIC during the summer. Compared to CMST, the additional assimilation of summer SIT leads to an SIT distribution that is more similar to that from CryoSat-2 (Figures 2a-2c). The overestimation of the ice thickness by CMST is corrected particularly in the Fram Strait and in the Arctic Ocean

on the northern coast of the Canadian Arctic Archipelago and Greenland. These are regions where the sea ice experiences strong deformation and the ice surface is roughest (Farrell et al., 2020; Kwok, 2015). Further, our results demonstrate relatively strong agreement with observed SIE and SIV during the entire summer season (Figures 2d-2e), both during the ice melting phase and freezing timing (mid-September).

Root-mean-square error (RMSE), mean bias (MB), and correlation coefficient (CC), whose calculation methods are described in Text S2 in Supporting Information S1, are used to quantify comparisons between CMST, ANA, and observations. The CCs for SIE and SIV between ANA/CMST and observations are nearly equal. Statistically, the CC for SIE between ANA and NSIDC data is ~1, while for SIV, it is 0.97 between ANA and CryoSat-2 data. The RMSE for SIE calculated from ANA and observations is roughly 0.72×10^6 km^2, although it is somewhat bigger when calculated using CMST and observations, where it is 0.74×10^6 km^2. In relation to the SIV calculated by CMST and ANA, the RMSEs are likewise decreased from 2.43×10^3 km^3 to 1.97×10^3 km^3, demonstrating that the further assimilation of summer SIT improves the estimates for both SIE and SIV. We notice that the initial state from CMST still exhibits a large error in estimating SIV even though it has assimilated SIT and SIC throughout the cold season and assimilated SIC during the summer season. Besides, we hypothesize that there are two reasons why there is still a significant misfit between ANA and CryoSat-2 until the end of June. First, the DA system takes a certain period to spin up itself before leading to consistent improvements (Mu, Yang, et al., 2018). Second, around the end of May and June, CryoSat-2 exhibits substantially higher uncertainty than the model state, bringing our ANA closer to the model state.

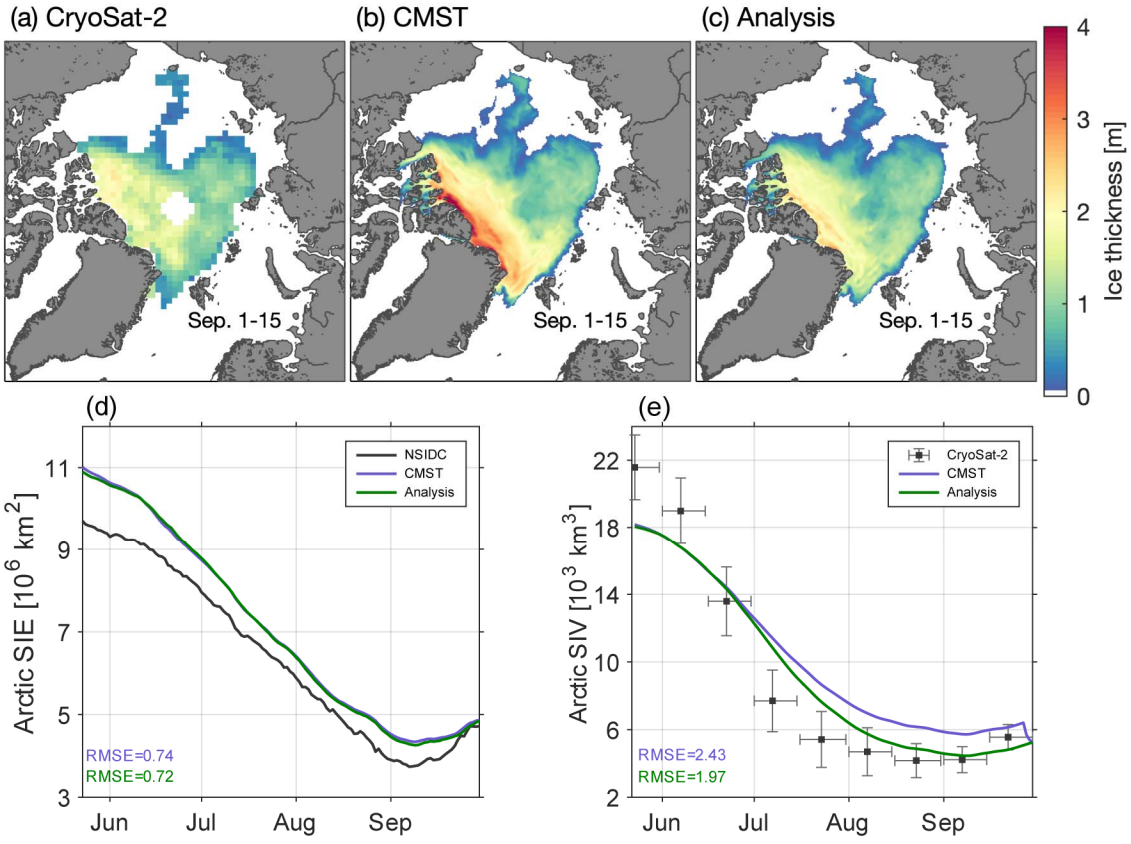

Figure 2. Arctic sea-ice thickness averaged over September 1-15, 2016 from CryoSat-2, Combined Model and Satellite Thickness (CMST) and Analysis (ANA) are shown in (a), (b) and (c). Panels (d) and (e) present the developments of summer sea-ice extent (SIE) and volume (SIV), respectively. The vertical bar in (e) for CryoSat-2 is for uncertainty and the horizontal bar is the time span for biweekly CryoSat-2 data. Root-mean-square errors (RMSEs) shown in purple and green are for CMST against observations and ANA against observations, respectively.

Because the sea-ice model's parameterizations are imperfect and satellite measurements of ice thickness have significant uncertainties in coastal areas of thick MYI, the CMST analysis is most uncertain around the northern coast of the Canadian Arctic Archipelago and Greenland (Mu, Losch, et al., 2018). Comparisons between ANA, CMST, CryoSat-2, and airborne sea ice surveys (Figure 3) are conducted to determine differences in certain places where strong sea-ice deformation occurs. As shown in Figure 2b, CMST appears to estimate excessively thick ice in these regions, whereas CryoSat-2 measures thinner sea ice than airborne surveys, as shown in

Landy et al. (2022). The median values of airborne surveys, CMST and CryoSat-2 are 1.58 m, 2.33 m and 0.9 m, respectively. With a median of 1.86 m, which is closest to that of the airborne surveys, ANA has the best agreement among CryoSat-2, CMST, and ANA. This likewise holds for the dominating probability density estimates for the observed and simulated SIT. The best agreement between airborne surveys and ANA is also verified by their lower and upper quartiles. Benefiting from the model dynamics and summer SIT assimilation, our ANA has reduced the overestimation of ice thickness in CMST, particularly in the Arctic coasts of north Greenland, while preventing the underestimation evident in CryoSat-2 observations.

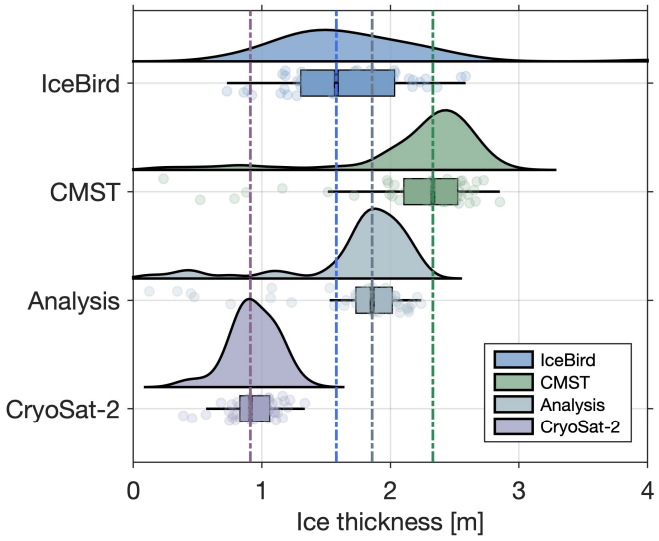

Figure 3. Comparison between observed sea-ice thickness (SIT) from the airborne surveys (IceBird) and CryoSat-2, simulated SIT from the Combined Model and Satellite Thickness (CMST) and Analysis (ANA). The raincloud plots show the distributions of observed and simulated SIT and their key summary statistics (i.e., lower and upper quartiles, medians, and outliers). The medians for IceBird observations, CMST, ANA and CryoSat-2 are represented by blue, green, gray and violet dashed lines, respectively. Translucent dots represent the observed and simulated SIT exactly.

With sea-ice observations from BGEP moorings, the performance of CryoSat-2, CMST and ANA are assessed in the Beaufort Sea (Figure 4, Tables 1 and Table S1 in Supporting Information S1). The three datasets replicate the SIT developments that were measured by in-situ measurements (Figures 4a-4c). Compared to BGEP moorings, both CMST and ANA show comparatively small RMSE and MB. For the BGEP measurements, the RMSEs for ANA are up

to 0.05 m smaller than for CMST, while the MB is generally below 0.10 m and differs by up to 0.06 m, indicating that the further assimilation of CryoSat-2 improves not only the estimate of Arctic SIV but also the local SIT. It should be noted that the growth in SIT at the location of BGEP_B during mid- to late-September (Fig. 4b) is only well captured by ANA, which integrates model dynamics with satellite SIT.

Compared to AWI ADCPs (i.e., Vilk1-14 and Vilk3-14) deployed in the Laptev Sea, CryoSat-2, CMST and ANA have relatively larger deviations (Figures 4d-4e). The RMSEs for ANA versus Vilk1-14 and Vilk3-14 are 0.61 m and 0.78 m while the MBs are –0.39 m and –0.43 m. Although the SIT as measured by AWI ADCPs is underestimated by our model outputs, the MB for ANA is within the AWI ADCPs' uncertainty (±0.96 m). Further, the CryoSat-2 data shows an even larger underestimation. However, in contrast to the BGEP time series, the evolution of the SIT at the Vilk moorings was complex during summer 2016. The ice cover actually thickened between the start and end of the summer as highly-deformed ice was transiting the mooring locations (Belter et al., 2020). This demonstrates that ANA still functions in the Laptev Sea. Since the Laptev Sea is a crucial sea area affecting navigation safety (e.g., Min et al., 2022; Min et al., 2023), both observations and model simulations need to be further optimized for sea ice conditions in unusual years like 2016.

Table 1. Main statistics [m] used to verify the sea-ice thickness of the Combined Model and Satellite Thickness (CMST) and Analysis (ANA) against in-situ measurements (i.e., BGEP_A, BGEP_B, BGEP_D, Vilk1-14 and Vilk3-14) over the summer period in 2016.

In-situ observation	RMSE		MB	
	CMST	ANA	CMST	ANA
BGEP_A	0.35	0.35	0.08	0.07
BGEP_B	0.24	0.23	0.01	–0.05
BGEP_D	0.40	0.35	0.09	0.03
Vilk1-14	0.61	0.61	–0.40	–0.39
Vilk3-14	0.76	0.78	–0.45	–0.43

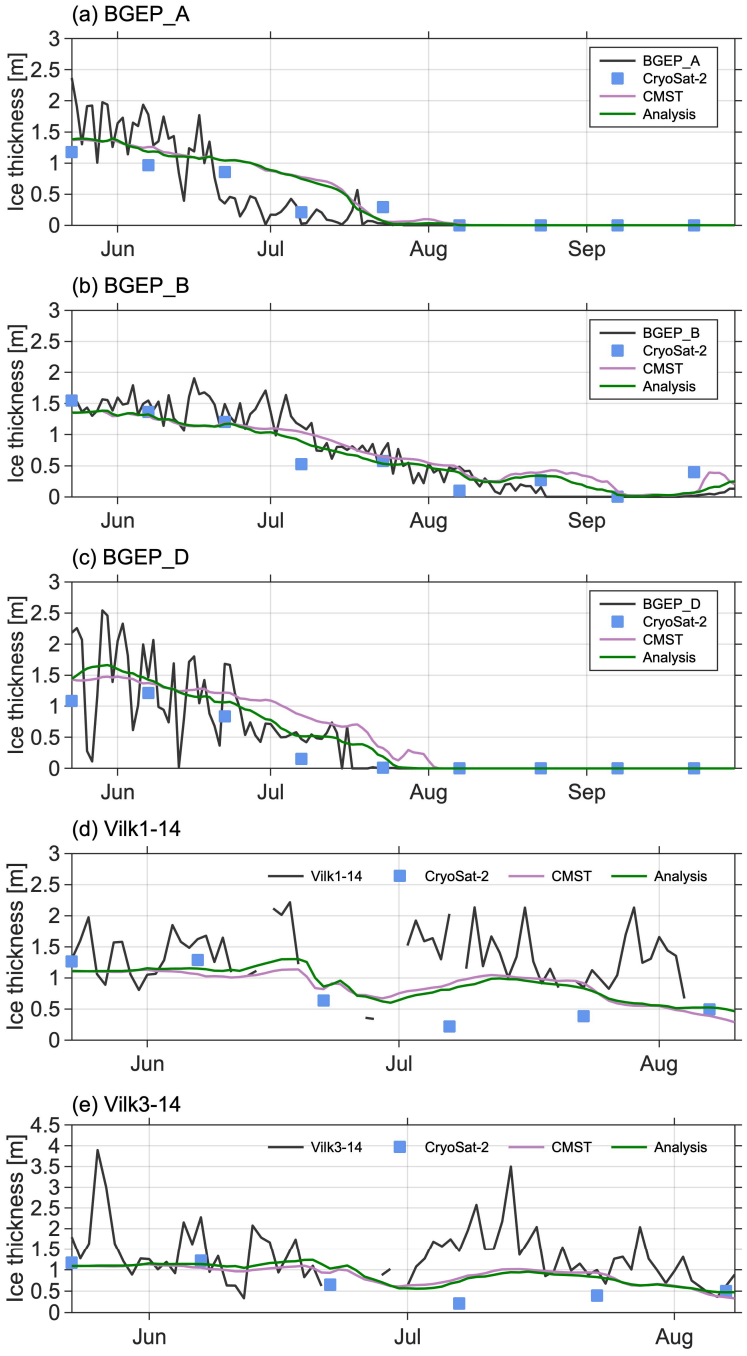

Figure 4. Comparison of summer sea-ice thickness (SIT) from the Beaufort Gyre Exploration Program (BGEP) moorings, CryoSat-2, Combined Model and Satellite Thickness (CMST) and Analysis (ANA), during summer 2016. (a, b and c) are for SIT developments at BGEP_A, BGEP_B and BGEP_D. Panels (d) and (e) are for SIT developments at AWI Acoustic Doppler Current Profiler (ADCP) sensor deployments (Vilk1-14 and Vilk3-14) in the Laptev Sea.

4 Conclusions and discussions

To investigate the impact of assimilating the recent CryoSat-2 summer SIT in estimating Arctic summer SIT, we have carried out a DA experiment including a novel IAU approach. This method guarantees a gradual development of the sea-ice fields over time while allowing the assimilation of the infrequent summer SIT data, which is only provided on a two-week basis, in conjunction with the daily SIC data. The model dynamics play an important role in the assimilation and have the potential to reduce the underestimation of SIT in satellite retrievals, especially along the Arctic coasts of Greenland (Landy et al., 2022), where the ice thermodynamically thickens as well as experiences deformation over many winter seasons (Kwok, 2015; Tschudi et al., 2016). Likewise, our ANA basically solves the overestimation of SIT estimated by CMST in those areas and thus provides a more reliable estimate of summer SIT. Moreover, in comparison to the CMST reanalysis, which did not assimilate this summer SIT data, the evolution of the SIV estimates agrees better with that derived from CryoSat-2.

These findings demonstrate the benefits of assimilating CryoSat-2 summer SIT for estimating Arctic sea ice and hence improving the initial states for sea-ice forecasts. As a result, the sea-ice forecast, which is highly relevant for marine activities, can benefit greatly from the enhanced initial states (Xiu et al., 2022; Yang et al., 2019). Further, our IAU assimilation scheme can be well applied to summer sea ice assimilation, which is important for developing a sea-ice reanalysis that assimilates year-round satellite ice thickness and concentration. A continuous long-term ice thickness record with a finer temporal-spatial resolution that assimilates both year-round SIC and SIT will be reconstructed in the future.

Acknowledgments

This study contributes to the Year of Polar Prediction, a flagship activity of the Polar Prediction Project, initiated by the World Weather Research Programme of the World Meteorological Organization. This study was funded by the National Natural Science Foundation of China (No. 41922044, 41941009), the National Key R&D Program of China (No. 2022YFE0106300), the Guangdong Basic and Applied Basic Research Foundation (No. 2020B1515020025), and the fundamental research funds for the Norges Forskningsråd. (No. 328886). C. Min acknowledges support from the China Scholarship Council (No. 202006380131). N. Mamnun acknowledges funding support from the Helmholtz Initiative and Networking Fund pilot project Uncertainty

Quantification – From Data to Reliable Knowledge (Helmholtz-UQ). We acknowledge the computing resources on the compute cluster Ollie provided by the Alfred Wegener Institute Helmholtz Centre for Polar and Marine Research and computing resources provided by National Supercomputer Center in Guangzhou. We thank the National Snow and Ice Data Center and the University of Hamburg for providing the SIC data, the European Centre for Medium-Range Weather Forecasts for the UKMO ensemble forecasting data, and the Woods Hole Oceanographic Institution for the BGEP ULS-measured sea-ice draft data.

Open Research

All data used in this study are openly accessible. The BGEP ULS-measured sea-ice draft data were downloaded from https://www2.whoi.edu/site/beaufortgyre/data/mooring-data/. The sea-ice draft data measured by AWI ADCP sensors were downloaded from https://doi.pangaea.de/10.1594/PANGAEA.912927. The SIC data provided by the National Snow and Ice Data Center and the University of Hamburg are available at https://nsidc.org/data/nsidc-0051/versions/2 and https://www.cen.uni-hamburg.de/en/icdc/data/, respectively. The UKMO ensemble forecasting data were obtained from the THORPEX Interactive Grand Global Ensemble (TIGGE) archive (https://apps.ecmwf.int/datasets/data/tigge/levtype=sfc/type=cf/). The CryoSat-2 SIT data is available from the British Antarctic Survey Polar Data Centre at https://doi.org/10.5285/D8C66670-57AD-44FC-8FEF-942A46734ECB. The MITgcm model code is available at http://mitgcm.org. PDAF can be obtained from http://pdaf.awi.de.

References

Bailey, H., Hubbard, A., Klein, E. S., Mustonen, K.-R., Akers, P. D., Marttila, H., & Welker, J. M. (2021). Arctic sea-ice loss fuels extreme European snowfall. *Nature Geoscience, 14*(5), 283-288. https://doi.org/10.1038/s41561-021-00719-y

Belter, H. J., Krumpen, T., Hendricks, S., Hoelemann, J., Janout, M. A., Ricker, R., & Haas, C. (2020). Satellite-based sea ice thickness changes in the Laptev Sea from 2002 to 2017: comparison to mooring observations. *The Cryosphere, 14*(7), 2189-2203. https://doi.org/10.5194/tc-14-2189-2020

Belter, H. J., Krumpen, T., Janout, M. A., Ross, E., & Haas, C. (2021). An Adaptive Approach to Derive Sea Ice Draft from Upward-Looking Acoustic Doppler Current Profilers (ADCPs), Validated by Upward-Looking Sonar (ULS) Data. *Remote Sensing, 13*(21). https://doi.org/10.3390/rs13214335

Blockley, E. W., & Peterson, K. A. (2018). Improving Met Office seasonal predictions of Arctic sea ice using assimilation of CryoSat-2 thickness. *The Cryosphere, 12*(11), 3419-3438. https://doi.org/10.5194/tc-12-3419-2018

Bloom, S. C., Takacs, L. L., da Silva, A. M., & Ledvina, D. (1996). Data Assimilation Using Incremental Analysis Updates. *Monthly Weather Review, 124*(6), 1256-1271. https://doi.org/10.1175/1520-0493(1996)124<1256:DAUIAU>2.0.CO;2

Bowler, N. E., Arribas, A., Mylne, K. R., Robertson, K. B., & Beare, S. E. (2008). The MOGREPS short-range ensemble prediction system. *Quarterly Journal of the Royal Meteorological Society, 134*(632), 703-722. https://doi.org/10.1002/qj.234

Chylek, P., Folland, C., Klett, J. D., Wang, M., Hengartner, N., Lesins, G., & Dubey, M. K. (2022). Annual Mean Arctic Amplification 1970–2020: Observed and Simulated by CMIP6 Climate Models. *Geophysical Research Letters, 49*(13), e2022GL099371. https://doi.org/10.1029/2022GL099371

Cohen, J., Agel, L., Barlow, M., Garfinkel, C. I., & White, I. (2021). Linking Arctic variability and change with extreme winter weather in the United States. *Science, 373*(6559), 1116-1121. https://doi.org/10.1126/science.abi9167

Comiso, J. C., Cavalieri, D. J., Parkinson, C. L., & Gloersen, P. (1997). Passive microwave algorithms for sea ice concentration: A comparison of two techniques. *Remote Sensing of Environment, 60*(3), 357-384. https://doi.org/10.1016/S0034-4257(96)00220-9

Dawson, G., Landy, J., Tsamados, M., Komarov, A. S., Howell, S., Heorton, H., & Krumpen, T. (2022). A 10-year record of Arctic summer sea ice freeboard from CryoSat-2. *Remote Sensing of Environment, 268*, 112744. https://doi.org/10.1016/j.rse.2021.112744

Day, J. J., Hawkins, E., & Tietsche, S. (2014). Will Arctic sea ice thickness initialization improve seasonal forecast skill? *Geophysical Research Letters, 41*(21), 7566-7575. https://doi.org/10.1002/2014GL061694

DiGirolamo, N., Parkinson, C. L., Cavalieri, D. J., Gloersen, P., & Zwally, H. J. (2022). Sea Ice Concentrations from Nimbus-7 SMMR and DMSP SSM/I-SSMIS Passive Microwave Data*, Version 2 [Data Set],* https://doi.org/10.5067/MPYG15WAA4WX.

Eicken, H. (2013). Arctic sea ice needs better forecasts. *Nature, 497*(7450), 431-433. https://doi.org/10.1038/497431a

Farrell, S. L., Duncan, K., Buckley, E. M., Richter-Menge, J., & Li, R. (2020). Mapping Sea Ice Surface Topography in High Fidelity With ICESat-2. *Geophysical Research Letters, 47*(21), e2020GL090708. https://doi.org/10.1029/2020GL090708

Gaspari, G., & Cohn, S. E. (1999). Construction of correlation functions in two and three dimensions. *Quarterly Journal of the Royal Meteorological Society, 125*(554), 723-757. https://doi.org/10.1002/qj.49712555417

Hibler, W. D. (1979). A Dynamic Thermodynamic Sea Ice Model. *Journal of Physical Oceanography, 9*(4), 815-846. https://doi.org/10.1175/1520-0485(1979)009<0815:ADTSIM>2.0.CO;2

Kaleschke, L., Tian-Kunze, X., Maaß, N., Mäkynen, M., & Drusch, M. (2012). Sea ice thickness retrieval from SMOS brightness temperatures during the Arctic freeze-up period. *Geophysical Research Letters, 39*(5). https://doi.org/10.1029/2012GL050916

Kaleschke, L., Lupkes, C., Vihma, T., Haarpaintner, J., Bochert, A., Hartmann, J., & Heygster, G. (2001). SSM/I sea ice remote sensing for mesoscale ocean-atmosphere interaction analysis. *Canadian Journal of Remote Sensing, 27*(5), 526-537. https://doi.org/10.1080/07038992.2001.10854892

Kern, S., Kaleschke, L., & Spreen, G. (2010). Climatology of the Nordic (Irminger, Greenland, Barents, Kara and White/Pechora) Seas ice cover based on 85 GHz satellite microwave radiometry: 1992–2008. *Tellus A: Dynamic Meteorology and Oceanography, 62*(4), 411-434. http://doi.org/10.1111/j.1600-0870.2009.00457.x

Krumpen, T., Belter, H. J., Boetius, A., Damm, E., Haas, C., Hendricks, S., et al. (2019). Arctic warming interrupts the Transpolar Drift and affects long-range transport of sea ice and ice-rafted matter. Scientific Reports, 9(1), 5459. https://doi.org/10.1038/s41598-019-41456-y

Krumpen, T., Birrien, F., Kauker, F., Rackow, T., von Albedyll, L., Angelopoulos, M., et al. (2020). The MOSAiC ice floe: sediment-laden survivor from the Siberian shelf. The Cryosphere, 14(7), 2173-2187. https://doi.org/10.5194/tc-14-2173-2020

Kwok, R. (2015). Sea ice convergence along the Arctic coasts of Greenland and the Canadian Arctic Archipelago: Variability and extremes (1992–2014). *Geophysical Research Letters, 42*(18), 7598-7605. https://doi.org/10.1002/2015GL065462

Kwok, R. (2018). Arctic sea ice thickness, volume, and multiyear ice coverage: losses and coupled variability (1958–2018). *Environmental Research Letters, 13*(10), 105005. https://doi.org/10.1088/1748-9326/aae3ec

Kwok, R., Kacimi, S., Webster, M. A., Kurtz, N. T., & Petty, A. A. (2020). Arctic Snow Depth and Sea Ice Thickness From ICESat-2 and CryoSat-2 Freeboards: A First Examination. *Journal of Geophysical Research: Oceans, 125*(3), e2019JC016008. https://doi.org/10.1029/2019JC016008

Landy, J. C., Tsamados, M., & Scharien, R. K. (2019). A Facet-Based Numerical Model for Simulating SAR Altimeter Echoes From Heterogeneous Sea Ice Surfaces. *IEEE Transactions on Geoscience and Remote Sensing, 57*(7), 4164-4180. https://doi.org/10.1029/2008JC004753

Landy, J. C., Petty, A. A., Tsamados, M., & Stroeve, J. C. (2020). Sea Ice Roughness Overlooked as a Key Source of Uncertainty in CryoSat-2 Ice Freeboard Retrievals. *Journal of Geophysical Research: Oceans, 125*(5), e2019JC015820. https://doi.org/10.1029/2019JC015820

Landy, J. C., Dawson, G. J., Tsamados, M., Bushuk, M., Stroeve, J. C., Howell, S. E. L., et al. (2022). A year-round satellite sea-ice thickness record from CryoSat-2. *Nature*. https://doi.org/10.1038/s41586-022-05058-5

Lavergne, T., Sørensen, A. M., Kern, S., Tonboe, R., Notz, D., Aaboe, S., et al. (2019). Version 2 of the EUMETSAT OSI SAF and ESA CCI sea-ice concentration climate data records. *The Cryosphere, 13*(1), 49-78. https://doi.org/10.5194/tc-13-49-2019

Lawrence, I. R., Armitage, T. W. K., Tsamados, M. C., Stroeve, J. C., Dinardo, S., Ridout, A. L., et al. (2021). Extending the Arctic sea ice freeboard and sea level record with the Sentinel-3 radar altimeters. *Advances in Space Research, 68*(2), 711-723. https://doi.org/10.1016/j.asr.2019.10.011

458 Laxon, S. W., Giles, K. A., Ridout, A. L., Wingham, D. J., Willatt, R., Cullen, R., et al. (2013).
459 CryoSat-2 estimates of Arctic sea ice thickness and volume. *Geophysical Research*
460 *Letters, 40*(4), 732-737. https://doi.org/10.1002/grl.50193
461 Lellouche, J. M., Le Galloudec, O., Drévillon, M., Régnier, C., Greiner, E., Garric, G., et al.
462 (2013). Evaluation of global monitoring and forecasting systems at Mercator Océan.
463 *Ocean Sci., 9*(1), 57-81. https://doi.org/10.5194/os-9-57-2013
464 Li, X., Yang, Q., Yu, L., Holland, P. R., Min, C., Mu, L., & Chen, D. (2022). Unprecedented
465 Arctic sea ice thickness loss and multiyear-ice volume export through Fram Strait during
466 2010–2011. *Environmental Research Letters, 17*(9), 095008.
467 https://doi.org/10.1088/1748-9326/ac8be7
468 Liu, J., Song, M., Zhu, Z., Horton, R. M., Hu, Y., & Xie, S.-P. (2022). Arctic sea-ice loss is
469 projected to lead to more frequent strong El Niño events. *Nature Communications, 13*(1),
470 4952. https://doi.org/10.1038/s41467-022-32705-2
471 Losch, M., Menemenlis, D., Campin, J.-M., Heimbach, P., & Hill, C. (2010). On the formulation
472 of sea-ice models. Part 1: Effects of different solver implementations and
473 parameterizations. *Ocean Modelling, 33*(1), 129-144.
474 https://doi.org/10.1016/j.ocemod.2009.12.008
475 Marshall, J., Adcroft, A., Hill, C., Perelman, L., & Heisey, C. (1997). A finite-volume,
476 incompressible Navier Stokes model for studies of the ocean on parallel computers.
477 *Journal of Geophysical Research: Oceans, 102*(C3), 5753-5766.
478 https://doi.org/10.1029/96JC02775
479 Massonnet, F., Fichefet, T., & Goosse, H. (2015). Prospects for improved seasonal Arctic sea ice
480 predictions from multivariate data assimilation. *Ocean Modelling, 88*, 16-25.
481 https://doi.org/10.1016/j.ocemod.2014.12.013
482 Melling, H., Johnston, P. H., & Riedel, D. A. (1995). Measurements of the Underside
483 Topography of Sea-Ice by Moored Subsea Sonar. *Journal of Atmospheric and Oceanic*
484 *Technology, 12*(3), 589-602. https://doi.org/10.1175/1520-
485 0426(1995)012<0589:MOTUTO>2.0.CO;2
486 Mignac, D., Martin, M., Fiedler, E., Blockley, E., & Fournier, N. (2022). Improving the Met
487 Office's Forecast Ocean Assimilation Model (FOAM) with the assimilation of satellite-
488 derived sea-ice thickness data from CryoSat-2 and SMOS in the Arctic. *Quarterly*

Journal of the Royal Meteorological Society, 148(744), 1144-1167. https://doi.org/10.1002/qj.4252

Min, C., Mu, L., Yang, Q., Ricker, R., Shi, Q., Han, B., et al. (2019). Sea ice export through the Fram Strait derived from a combined model and satellite data set. *The Cryosphere, 13*(12), 3209-3224. https://doi.org/10.5194/tc-13-3209-2019

Min, C., Yang, Q., Mu, L., Kauker, F., & Ricker, R. (2021). Ensemble-based estimation of sea-ice volume variations in the Baffin Bay. *The Cryosphere, 15*(1), 169-181. https://doi.org/10.5194/tc-15-169-2021

Min, C., Yang, Q., Chen, D., Yang, Y., Zhou, X., Shu, Q., & Liu, J. (2022). The Emerging Arctic Shipping Corridors. *Geophysical Research Letters, 49*(10), e2022GL099157. https://doi.org/10.1029/2022GL099157

Min, C., Zhou, X., Luo, H., Yang, Y., Wang, Y., Zhang, J., & Yang, Q. (2023). Toward Quantifying the Increasing Accessibility of the Arctic Northeast Passage in the Past Four Decades. *Advances in Atmospheric Sciences*. https://doi.org/10.1007/s00376-022-2040-3

Mu, L., Losch, M., Yang, Q., Ricker, R., Losa, S. N., & Nerger, L. (2018). Arctic-Wide Sea Ice Thickness Estimates From Combining Satellite Remote Sensing Data and a Dynamic Ice-Ocean Model with Data Assimilation During the CryoSat-2 Period. *Journal of Geophysical Research: Oceans, 123*(11), 7763-7780. https://doi.org/10.1029/2018JC014316

Mu, L., Yang, Q., Losch, M., Losa, S. N., Ricker, R., Nerger, L., & Liang, X. (2018). Improving sea ice thickness estimates by assimilating CryoSat-2 and SMOS sea ice thickness data simultaneously. *Quarterly Journal of the Royal Meteorological Society, 144*(711), 529-538. https://doi.org/10.1002/qj.3225

Nerger, L., & Hiller, W. (2013). Software for ensemble-based data assimilation systems—Implementation strategies and scalability. *Computers & Geosciences, 55*, 110-118. https://doi.org/10.1016/j.cageo.2012.03.026

Nerger, L., Janjić, T., Schröter, J., & Hiller, W. (2012). A Unification of Ensemble Square Root Kalman Filters. *Monthly Weather Review, 140*(7), 2335-2345. https://doi.org/10.1175/MWR-D-11-00102.1

Nguyen, A. T., Menemenlis, D., & Kwok, R. (2011). Arctic ice-ocean simulation with optimized model parameters: Approach and assessment. *Journal of Geophysical Research-Oceans, 116*. https://doi.org/10.1029/2010JC006573

Ourmières, Y., Brankart, J. M., Berline, L., Brasseur, P., & Verron, J. (2006). Incremental Analysis Update Implementation into a Sequential Ocean Data Assimilation System. *Journal of Atmospheric and Oceanic Technology, 23*(12), 1729-1744. https://doi.org/10.1175/JTECH1947.1

Park, Y. Y., Buizza, R., & Leutbecher, M. (2008). TIGGE: Preliminary results on comparing and combining ensembles. *Quarterly Journal of the Royal Meteorological Society, 134*(637), 2029-2050. https://doi.org/10.1002/qj.334

Parkinson, C. L., & Washington, W. M. (1979). A large-scale numerical model of sea ice. *Journal of Geophysical Research: Oceans, 84*(C1), 311-337. https://doi.org/10.1029/JC084iC01p00311

Petty, A. A., Kurtz, N. T., Kwok, R., Markus, T., & Neumann, T. A. (2020). Winter Arctic Sea Ice Thickness From ICESat-2 Freeboards. *Journal of Geophysical Research: Oceans, 125*(5), e2019JC015764. https://doi.org/10.1029/2019JC015764

Petty, A. A., Stroeve, J. C., Holland, P. R., Boisvert, L. N., Bliss, A. C., Kimura, N., & Meier, W. N. (2018). The Arctic sea ice cover of 2016: a year of record-low highs and higher-than-expected lows. *The Cryosphere, 12*(2), 433-452. https://doi.org/10.5194/tc-12-433-2018

Petty, A. A., Schröder, D., Stroeve, J. C., Markus, T., Miller, J., Kurtz, N. T., et al. (2017). Skillful spring forecasts of September Arctic sea ice extent using passive microwave sea ice observations. *Earth's Future, 5*(2), 254-263. https://doi.org/10.1002/2016EF000495

Pfaffling, A., Haas, C., & Reid, J. E. (2007). Direct helicopter EM - Sea-ice thickness inversion assessed with synthetic and field data. *Geophysics, 72*(4), F127-F137. https://doi.org/10.1190/1.2732551

Qi, D., Ouyang, Z., Chen, L., Wu, Y., Lei, R., Chen, B., et al. (2022). Climate change drives rapid decadal acidification in the Arctic Ocean from 1994 to 2020. *Science, 377*(6614), 1544-1550. https://doi.org/10.1126/science.abo0383

Rantanen, M., Karpechko, A. Y., Lipponen, A., Nordling, K., Hyvärinen, O., Ruosteenoja, K., et al. (2022). The Arctic has warmed nearly four times faster than the globe since 1979.

549 *Communications Earth & Environment, 3*(1), 168. https://doi.org/10.1038/s43247-022-
550 00498-3
551 Ricker, R., Hendricks, S., Helm, V., Skourup, H., & Davidson, M. (2014). Sensitivity of
552 CryoSat-2 Arctic sea-ice freeboard and thickness on radar-waveform interpretation. *The*
553 *Cryosphere, 8*(4), 1607-1622. https://doi.org/10.5194/tc-8-1607-2014
554 Semtner, A. J. (1976). A Model for the Thermodynamic Growth of Sea Ice in Numerical
555 Investigations of Climate. *Journal of Physical Oceanography, 6*(3), 379-389.
556 https://doi.org/10.1175/1520-0485(1976)006<0379:AMFTTG>2.0.CO;2
557 Spreen, G., Kaleschke, L., & Heygster, G. (2008). Sea ice remote sensing using AMSR-E 89-
558 GHz channels. *Journal of Geophysical Research: Oceans, 113*(C2).
559 https://doi.org/10.1029/2005JC003384
560 Stroeve, J., Liston, G. E., Buzzard, S., Zhou, L., Mallett, R., Barrett, A., et al. (2020). A
561 Lagrangian snow evolution system for sea ice applications (SnowModel-LG): Part II—
562 Analyses. Journal of Geophysical Research: Oceans, 125, e2019JC015900.
563 https://doi.org/10.1029/2019JC015900
564 Stroeve, J., & Notz, D. (2018). Changing state of Arctic sea ice across all seasons.
565 *Environmental Research Letters, 13*(10), 103001. https://doi.org/10.1088/1748-
566 9326/aade56
567 Tian-Kunze, X., Kaleschke, L., Maaß, N., Mäkynen, M., Serra, N., Drusch, M., & Krumpen, T.
568 (2014). SMOS-derived thin sea ice thickness: algorithm baseline, product specifications
569 and initial verification. *The Cryosphere, 8*(3), 997-1018. https://doi.org/10.5194/tc-8-997-
570 2014
571 Xie, J., Counillon, F., & Bertino, L. (2018). Impact of assimilating a merged sea-ice thickness
572 from CryoSat-2 and SMOS in the Arctic reanalysis. *The Cryosphere, 12*(11), 3671-3691.
573 https://doi.org/10.5194/tc-12-3671-2018
574 Xiu, Y., Luo, H., Yang, Q., Tietsche, S., Day, J., & Chen, D. (2022). The Challenge of Arctic
575 Sea Ice Thickness Prediction by ECMWF on Subseasonal Time Scales. *Geophysical*
576 *Research Letters, 49*(8), e2021GL097476. https://doi.org/10.1029/2021GL097476
577 Yang, Q., Losa, S. N., Losch, M., Jung, T., & Nerger, L. (2015). The role of atmospheric
578 uncertainty in Arctic summer sea ice data assimilation and prediction. *Quarterly Journal*

579 *of the Royal Meteorological Society, 141*(691), 2314-2323.
580 https://doi.org/10.1002/qj.2523
581 Yang, Q., Mu, L., Wu, X., Liu, J., Zheng, F., Zhang, J., & Li, C. (2019). Improving Arctic sea
582 ice seasonal outlook by ensemble prediction using an ice-ocean model. *Atmospheric*
583 *Research, 227*, 14-23. https://doi.org/10.1016/j.atmosres.2019.04.021
584 Yang, Q., Losa, S. N., Losch, M., Tian-Kunze, X., Nerger, L., Liu, J., et al. (2014). Assimilating
585 SMOS sea ice thickness into a coupled ice-ocean model using a local SEIK filter. *Journal*
586 *of Geophysical Research: Oceans, 119*(10), 6680-6692.
587 https://doi.org/10.1002/2014JC009963
588 Zhang, J., & Hibler, W. D. (1997). On an efficient numerical method for modeling sea ice
589 dynamics. *Journal of Geophysical Research: Oceans, 102*(C4), 8691-8702.
590 https://doi.org/10.1029/96JC03744
591 Zhou, X., Min, C., Yang, Y., Landy, J. C., Mu, L., & Yang, Q. (2021). Revisiting Trans-Arctic
592 Maritime Navigability in 2011–2016 from the Perspective of Sea Ice Thickness. *Remote*
593 *Sensing, 13*(14), 2766. https://doi.org/10.3390/rs13142766
594